BJR

https://doi.org/10.1259/bjr.20211096

Received: 30 September 2021 | Revised: 11 May 2022 | Accepted: 24 May 2022 | Published online: 28 June 2022

Cite this article as:
van Amerom JFP, Goolaub DS, Schrauben EM, Sun L, Macgowan CK, Seed M. Fetal cardiovascular blood flow MRI: techniques and applications. *Br J Radiol* (2023) 10.1259/bjr.20211096.

PRENATAL IMAGING ADVANCES: PHYSIOLOGY AND FUNCTION TO MOTION CORRECTION AND AI: REVIEW ARTICLE

Fetal cardiovascular blood flow MRI: techniques and applications

[1]JOSHUA FP VAN AMEROM, PhD, [1,2]DATTA SINGH GOOLAUB, PhD, [3]ERIC M SCHRAUBEN, PhD, [4,5]LIQUN SUN, MD, PhD, [1,2]CHRISTOPHER K MACGOWAN, PhD and [1,4,5,6]MIKE SEED, MD

[1]Division of Translational Medicine, SickKids Research Institute, Toronto, Canada
[2]Department of Medical Biophysics, University of Toronto, Toronto, Canada
[3]Department of Radiology & Nuclear Medicine, Amsterdam University Medical Centers, Amsterdam, Netherlands
[4]Division of Cardiology, Hospital for Sick Children, Toronto, Canada
[5]Department of Paediatrics, University of Toronto, Toronto, Canada
[6]Department of Diagnostic Imaging, Hospital for Sick Children, Toronto, Canada

Address correspondence to: Dr Joshua FP van Amerom
E-mail: *joshua.vanamerom@sickkids.ca*

ABSTRACT

Fetal cardiac MRI is challenging due to fetal and maternal movements as well as the need for a reliable cardiac gating signal and high spatiotemporal resolution. Ongoing research and recent technical developments to address these challenges show the potential of MRI as an adjunct to ultrasound for the assessment of the fetal heart and great vessels. MRI measurements of blood flow have enabled the assessment of normal fetal circulation as well as conditions with disrupted circulations, such as congenital heart disease, along with associated organ underdevelopment and hemodynamic instability. This review provides details of the techniques used in fetal cardiovascular blood flow MRI, including single slice and volumetric imaging sequences, post-processing and analysis, along with a summary of applications in human studies and animal models.

INTRODUCTION

Prenatal growth relies on healthy circulation to deliver oxygen and nutrients from the placenta to the fetal organs.[1] In conditions such as congenital heart disease and intrauterine growth restriction, prenatal circulatory disruption can lead to underdevelopment of the brain, lungs and the cardiovascular system itself, resulting in hemodynamic instability and organ injury during the transition to neonatal circulation.[2,3] Understanding of fetal circulation can contribute to prenatal diagnosis of these conditions and inform pre- and perinatal management.

Ultrasound is the primary modality for evaluating the fetal heart, including hemodynamic assessment.[4] However, quantification of volumetric blood flow using standard Doppler methods is subject to several sources of error that compromise accuracy[5–9] and recent advances in ultrasound transducer hardware and velocity estimation methods are still in the early stages of development.[10–12] MRI can play a role as a safe adjunct to ultrasound in the diagnosis of cardiovascular disease.[4,13] While challenges of motion, cardiac gating and achieving adequate spatiotemporal resolution have limited the clinical use of fetal cardiovascular MRI to date, ongoing research and technical developments show potential for evaluation of fetal cardiac morphology, function, oximetry and blood flow in the late second trimester through term.[14,15]

This article reviews the techniques commonly employed in MRI of fetal cardiovascular blood flow, including both single slice and volumetric imaging sequences, along with methods for post-processing and analysis. Applications in human studies and animal models are also summarized, and the article concludes with a discussion of strengths, limitations, and outlook.

BACKGROUND

Fetal cardiovascular circulation

The fetal cardiovascular system has shunts that allow for streaming of blood between structures that are normally isolated in the postnatal heart. These shunts, shown in Figure 1, include the ductus arteriosus (DA) that connects the main pulmonary artery (MPA) to the proximal descending aorta (DAo), and the foramen ovale (FO),

Figure 1. Human fetal circulatory system diagram. The foramen ovale, ductus arteriosus and ductus venosus allow for mixing of the systemic and pulmonary circulations. These shunts are open during fetal development and close at birth. Shading indicates blood oxygen saturation measured in late gestational age fetuses using MR oximetry. AAo, ascending aorta; abdo, abdomen; DAo, decscending aorta; DA, ductus arteriosus, DV, ductus venosus; FO, foramen ovale; GI, gastrointestinal system; IVC, inferior vena cava; LA, left atrium; LV, left ventricle; MPA, main pulmonary artery; PBF, pulmonary blood flow; RA, right atrium; RV, right ventricle; UA, umbilical arteries; UV, umbilical vein. Adapted with permission from *Ultrasound Obstet Gynecol* 2021; doi: 10.1002/uog.23707.

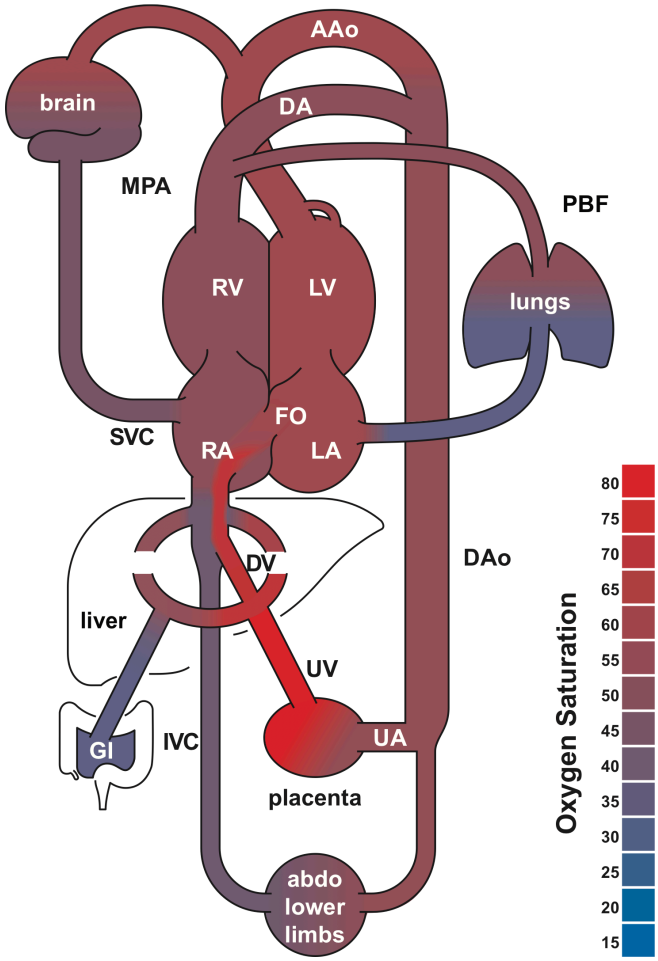

which allows oxygen rich blood from the placenta to stream from the umbilical vein (UV) through the ductus venosus (DV) and then across the atrial septum to the left side of the heart.[1] In combination with physiologic changes in the vasculature, these shunts allow for redistribution of blood to the brain either from the left heart, through the ascending aorta (AAo), or from the right heart as retrograde aortic arch flow, in conditions where flow is obstructed or the blood is hypoxic.[2,16] Blood returns to the heart from the brain and upper body by the superior vena cava (SVC).

At 32 weeks gestational age, in mid-third trimester, typical vessel diameters range from 4 mm in the DA and similarly sized right (RPA) and left pulmonary arteries (LPA) to 7 mm in the great arteries.[17–19] Normal fetal heart rates in the second half of gestation are usually in the range of 120–160 beats per minutes (bpm).[20]

Cardiac gating

Synchronization of data acquisition with the fetal cardiac cycle is essential for time-resolved flow MRI, however, the fetal electrocardiogram (ECG) signal is not reliable in the MR scanner environment. Two alternative methods are commonly used in fetal MRI.

Metric optimized gating

Retrospective image-based cardiac gating using entropy to measure data consistency was introduced as metric optimized gating (MOG) specifically for flow MRI in the fetus.[21] In this technique, data is temporally overacquired, to ensure full sampling of the lowest anticipated heart rate (*e.g.* 110 bpm), and then rearranged to reconstruct cine image series according to a parameterized model of the fetal heartbeat that minimizes the entropy metric in a region of pulsatile flow. Use of a multiparameter heart rate model that allows beat-to-beat variation[22] avoids flow errors that can occur with models that assume constant heart rates.[21] Fitting the heart rate model is usually performed as an offline post-processing step.

Doppler ultrasound gating

MR-compatible Doppler ultrasound (DUS) probes are being developed as an alternative to ECG in fetal MRI.[23–25] These non-imaging devices provide triggers based on Doppler waveforms of cardiac contraction and blood flow directly to the scanner for data synchronization, allowing for immediate online image reconstruction on the scanner system. DUS probe placement occurs during patient preparation at the start of the exam and re-positioning may be required if the fetal heart moves out of the acoustic field of the transducer.

Motion compensation

Maternal respiration and gross fetal motion can lead to movement of fetal cardiovascular anatomy within or through the imaging volume. Such movement corrupts the data leading to image artifact, however motion compensation techniques can be used to limit such detrimental effects. Two straightforward approaches are to scan in late gestation when gross fetal movement in the uterus becomes restricted or to use short scan durations in combination with maternal breath hold. Another approach is to use the data itself to track and correct for in-plane motion as well as identify and discard periods of through-plane movement.[26,27]

2D PHASE CONTRAST MR

Phase contrast (PC) MR is based on the accumulation of phase as blood flows through a magnetic field gradient. Making use of this mechanism, bipolar gradients are used to encode velocity along a given direction into the phase of the MR images. To account for non-velocity dependent contributions, a minimum of two measurements are needed with different flow sensitivities. They are then subtracted to yield a flow sensitive phase contrast image. Through-plane flow measurements are achieved by prescribing

Figure 2. Orientation of major fetal vessel cross-sectional slices in coronal, sagittal, and axial reference localizer images showing expected vessel arrangement in healthy human fetuses. AAo, ascending aorta; Ao, aorta; DAo, descending aorta; DA, ductus arteriosus; IVC, inferior vena cava; LPA, left pulmonary artery; LV, left ventricle; MPA, main pulmonary artery; RPA, right pulmonary artery; RV, right ventricle; SVC, superior vena cava; UV, umbilical vein. Figure and caption adapted with permission from MRI of Fetal and Maternal Diseases in Pregnancy. Springer, Cham. 2016. doi: 10.1007/978-3-319-21428-3_10.

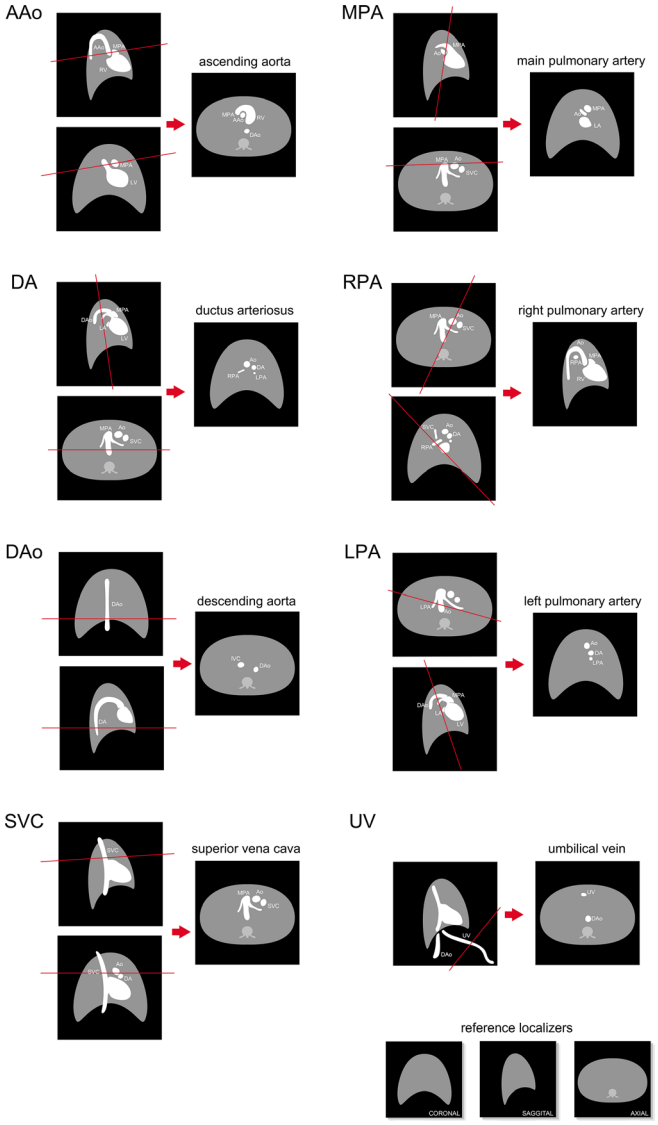

the imaging plane perpendicular to the axis of each vessel of interest. The velocity encoding gradient strength is set to reflect the maximum flow velocity being measured.

Fetal examinations using 2D PC MR require expert prescription of imaging planes cross-sectional to vessels of interest, as shown in Figure 2, and may involve repeating patient setup, localization or slice prescriptions when fetal movements occur. Figure 3 provides examples of flow curves in the major vessels measured by 2D PC MR in a healthy human fetus. Typical scan parameters, listed in Table 1, aim to balance competing goals of high spatio-temporal resolution, good signal-to-noise and short scan durations. The field of view must be sufficiently large to avoid spatial aliasing of maternal anatomy. In-plane voxel size should be 1.3 mm or less, as voxel size should be at most 1/3 the vessel diameter to avoid volume flow measurement errors from partial volume effects.[30] A temporal resolution of about 30 ms, or 15 cardiac phases, is usually used for time-resolved cine acquisitions which should be sufficient for accurate volume flow measurement,[31] though some high-frequency dynamic content of the blood flow may not be captured.[32] Accelerated imaging methods can be used to reduce scan duration by undersampling data and compensating with image reconstructions employing parallel imaging or compressed sensing. Encoding velocity should be set depending on the vessel of interest[33] (Table 1) as inappropriate selection of encoding velocity can lead to poor velocity to noise ratio and velocity underestimation.[34] Fetal cardiac MR is typically performed at 1.5 T as increased magnetic and radiofrequency field inhomogeneity at 3 T can lead to spatially localized signal loss, appearing as shading and banding artifacts.[35–38] However, the increased signal-to-noise at 3 T can improve visualization of small fetal vessels in 2D PC MR[39]

Cartesian K-space sampling

Cartesian sampling, commonly used in MRI, follows an efficient rectilinear grid through MR data acquisition k-space. A segmented acquisition can be used to collect data synchronized to the cardiac cycle over multiple heartbeats that are then reconstructed as cine image series with all data combined as a single cardiac cycle. In such a segmented acquisition, a subset of k-space lines is sampled repeatedly for an entire cardiac cycle and other subsets are collected during subsequent cardiac cycles. Non-triggered acquisitions can also be used, particularly to visualize flow direction[40,41] or assess flow in weakly pulsatile vessels,[42] however, care should be taken to avoid quantification errors when measuring pulsatile flows.[43,44]

The feasibility of cine 2D PC MR using Cartesian sampling with MOG has been established in studies of both pregnant and non-pregnant volunteers, which showed good reproducibility and interobserver agreement.[21,33,45] In a validation study using an MR-compatible exercise bike to increase adult heart rates to fetal range, good agreement and minimal bias were found between MOG and conventionally gated PC MR[33] Similarly, an independent validation using a pulsatile flow phantom showed good agreement between MOG and directly gated PC MR and confirmed previous intra- and interobserver variability results, but identified low velocity-to-noise as a potential cause for MOG misgating leading to underestimation of peak velocities.[34]

Fetal PC MR has also been successful with DUS-based cardiac gating, showing high interobserver agreement and good reproducibility of DUS-gated cine PC MR in fetal sheep and human fetuses.[46,47] DUS-based PC MR measurements of peak velocity in the human fetal descending aorta were highly correlated with Doppler ultrasound imaging measurements, though PC MR underestimated peak velocity as expected for the scan parameters used.[47] A study comparing DUS with MOG PC MR in human

Figure 3. Representative volume flow as a function of cardiac cycle in the major fetal vessels, measured by 2D PC MR in a healthy late-gestational age human fetus. AAo, ascending aorta; DAo, descending aorta; DA, ductus arteriosus; LPA, left pulmonary artery; MPA, main pulmonary artery; RPA, right pulmonary artery; SVC, superior vena cava; UV, umbilical vein. Reprinted under CC BY 2.0 from *J Cardiovasc Magn Reson* 2012;14(1):79. Caption adapted from original.

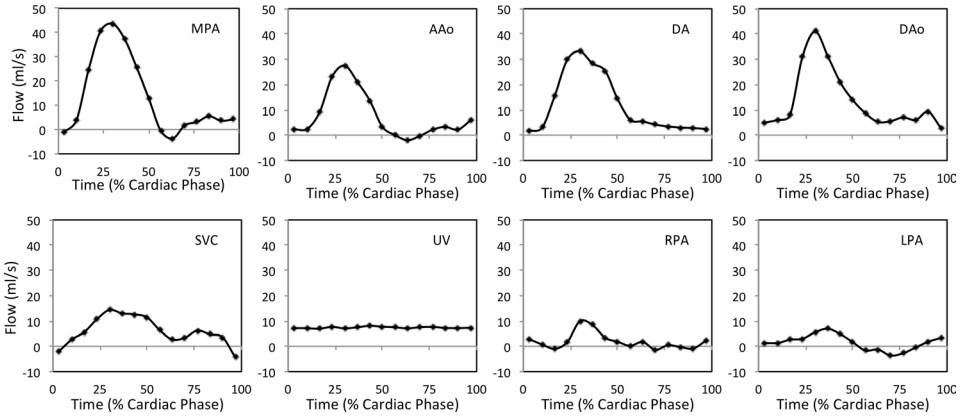

fetuses showed good agreement between descending aorta and umbilical vein flows measured using the two gating methods.[48]

Although Cartesian PC MR methods have been able to provide insight into fetal blood measurement, they are not robust to fetal motion.[49,50] In case of motion corruption, scans can be repeated, and probes may have to be repositioned.[29,47,49,50]

Golden angle radial K-space sampling

Golden angle radial k-space sampling uses trajectories in a stellate pattern with golden angle increments.[51] This allows for quasi-uniform k-space coverage over arbitrary temporal windows. In turn, real-time reconstructions are possible from undersampled subsets of the acquisition with compressed sensing. These

Table 1. Typical human fetal cardiovascular cine MR blood flow imaging parameters at 1.5 T.

Acquisition	Conventional 2D PC MR [28]	Radial 2D PC MR	4D Flow [29]
Trajectory	Cartesian	golden angle radial	Cartesian
TR/TE (ms)	5.3/2.9	5.9/3.6	3.0/2.0
Flip angle (degrees)	20	20	6
Velocity sensitivity	Through-plane	Through-plane	Fully encoded
Encoding velocity (cm/s)	150†, 100‡ or 50§	150†, 100‡ or 50§	120
Acceleration	GRAPPA, $R = 2$ ($R_{eff} = 1.7$)	CS, $R \geq 4$	SENSE, $R = 2–3$ CS SENSE, $R = 4–6$
Cardiac gating	MOG or DUS	MOG or DUS	DUS
Motion correction	–	Automatic, based on ROI	–
Maternal respiration	Free breathing	Free breathing	Shallow
Field of view (mm)	340 × 234 × 5	340 × 340 × 5	300 × 300 × 50
Acquired voxel size (mm)	1.3 × 1.3 × 5.0	1.3 × 1.3 × 5.0	2.5 ×2.5 × 2.5
Acquisition matrix	256 × 176 × 1	256 × 256 × 1	120 × 120 × 20
Segments	3	–	2–3
Reconstructed cardiac phases	15	15	20–30
Acquired temporal resolution (ms)	32	29*	24–36*
Signal averages	1	1	1–2
Scan duration (s)	14–19	18	120–180

† 150 cm/s encoding velocity used for large arteries: ascending and descending aorta, main pulmonary artery and ductus arteriosus; ‡ 100 cm/s encoding velocity used for branch pulmonary arteries and superior vena cava; § 50 cm/s encoding velocity used for umbilical vein; TE, excitation time; TR, repetition time; MOG, metric optimized gating; DUS, Doppler ultrasound; GRAPPA, generalized autocalibrating partial parallel acquisition; CS, compressed sensing; SENSE, sensitivity encoding; R, acceleration factor; R_{eff}, effective acceleration factor; ROI, region of interest; * additional temporal blurring depending on regularization in CS reconstruction

real-time images can be used for retrospective motion correction and image-based cardiac gating.[22,49] Reconstructions are performed in three major stages. First, real-time reconstructions with large temporal window (~370 ms) are used to identify and reject data corrupted by gross fetal movement and to correct for in-plane motion. Second, motion-corrected real-time reconstructions with short temporal window (~45 ms) are used to derive a fetal heart rate model. Third, motion-corrected and cardiac-gated data are reconstructed into cine PC MR image sequences. Through this approach, motion-robust through-plane flow reconstructions have been possible in human fetuses from accelerated measurements.[49,52] Moreover, by encoding velocity in three orthogonal dimensions and having a flow compensated acquisition in a single slice, the same approach allows for multi-dimensional intracardiac blood flow visualization.[22]

Impact of motion correction on flow quantification

Uncorrected motion occurring during a PC MR acquisition can corrupt the measurement in various ways. Reconstructed images may comprise data from several anatomical planes.[53] With spatial blurring and artifacts, such as ghosting and streaking, arising from motion corruption, vessels become less conspicuous such that flow quantification inaccuracies may occur due to erroneous vessel contours. The presence of motion corruption in the acquired data can also impact the efficacy of metrics used in imaged-based gating or self-gating methods which can result in cardiac synchronization errors.[21]

A recent study showed higher quality images and more accurate flow measurements are possible with retrospective motion-corrected compared with Cartesian PC MR[49] As summarized in Figure 4, simulations showed mean and peak flow were overestimated in images with uncorrected motion, and these errors were reduced to well within 5% for motion-corrected radial PC MR Furthermore, the area of vessel contours drawn on PC MR with uncorrected motion was overestimated, and this error was approximately twice as large in uncorrected Cartesian PC MR than in uncorrected radial PC MR. Similar vessel contour area

Figure 4. Impact of sampling and motion correction in simulated cine 2D phase contrast MR. (Top) Magnitude and velocity-sensitive phase contrast images of the upper great vessels based on adult reference data, simulated with Cartesian and golden angle radial k-space sampling under three motion states: none, small (±3 voxels displacement in each in-plane direction, approximately ±12% DAo diameter) and large (±5 voxels displacement,±20% DAo diameter). With large, uncorrected motion, identification of the DAo (arrows) boundary becomes more difficult but is ameliorated with motion correction. (Bottom) Mean and peak flow errors in the DAo. Vertical lines represent the standard deviation. Horizontal lines indicate significant differences. NS, not significant; *, $p \leq 0.05$; **, $p \leq 10^{-4}$; ***, $p \leq 10^{-8}$; DAo, descending aorta. Figure and caption adapted with permission from *J Magn Reson Imaging*. 2021;53(2).

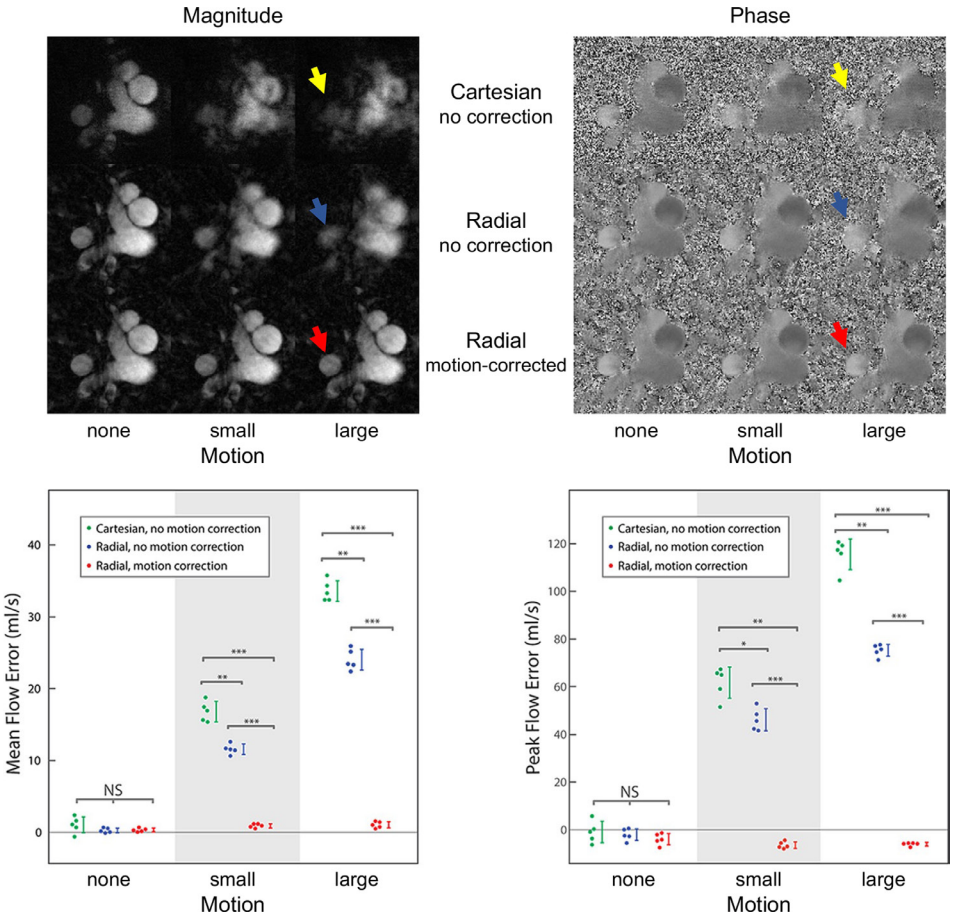

Figure 5. Cine phase contrast MR using Cartesian and motion-corrected golden angle radial sampling trajectories showing fetal three vessel view in systole. Mean and standard deviation of estimated in-plane displacement in the radial acquisition was 0.8 ± 0.5 mm with a maximum of 1.5 mm in images acquired with 1.3 mm resolution. Vessel labels are shown at left for reference. AAo, ascending aorta; MPA, main pulmonary artery; SVC, superior vena cava. Figure and caption adapted with permission from *J Magn Reson Imaging*. 2021;53(2).

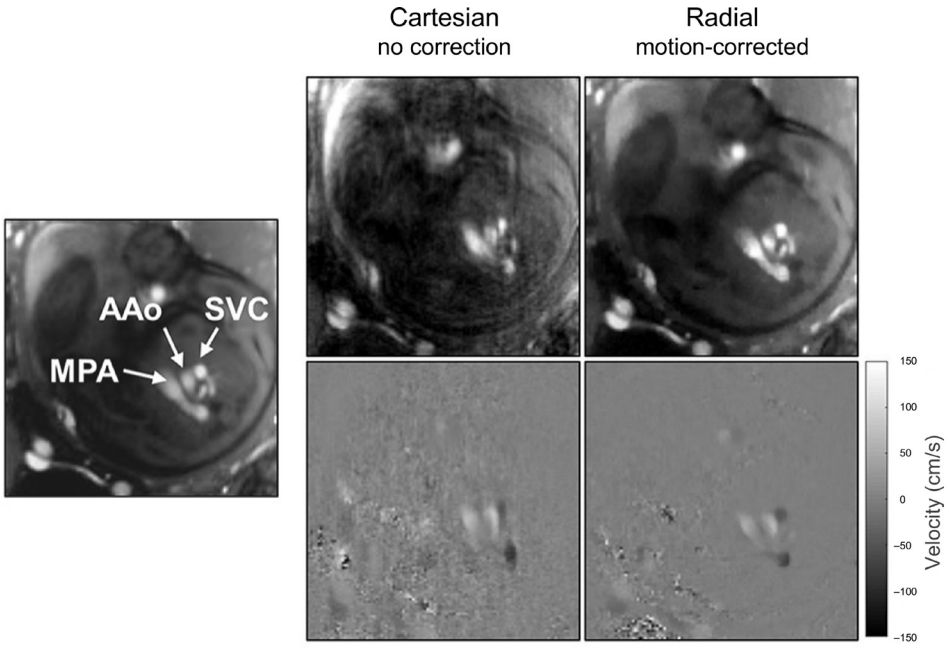

differences were found with *in vivo* measurements in late gestational age human fetuses. An example comparison in a human fetus is shown in Figure 5, with reduced image artifact and sharper vessel boundaries in the motion-corrected radial PC MR image. Overall, good agreement was found between *in vivo* measures of uncorrected Cartesian and motion-corrected radial PC MR flow measurements across a range of vessels, however, there was high variability and a small bias towards lower peak flows measured by motion-corrected radial PC MR. A subanalysis of that same data showed mean and peak flows were higher in uncorrected Cartesian PC MR with low image quality scores which were likely to be corrupted by motion compared to matched motion-corrected radial PC MR, in line with simulation results showing flow overestimation in the presence of motion. In addition, motion-robust acquisitions reduced the need to repeat acquisitions corrupted by brief in-plane movements.

4D FLOW MR

The extension of 2D PC MR to include volumetric coverage combined with the addition of flow sensitivity along all spatial dimensions is known as 4D flow MR.[54] The data from 4D flow MR consists of four volumetric data sets reconstructed over a representative cardiac cycle: one magnitude volume of the anatomy and three velocity volumes representing orthogonal velocity directions. This technique has been extensively studied as a research tool in adult and pediatric applications, namely in congenital heart diseases such as bicuspid aortic valve,[55,56] tetralogy of Fallot[57,58] and Marfan syndrome.[59,60] Its quantitative test–retest repeatability in large cardiac vessels relative to 2D PC MRI suggest it may be suitable for surveillance of heart disease and treatment decision-making.[61,62]

By virtue of the abundance of information gained from 4D flow MR, it should be well-suited to the task of assessing fetal cardiovascular hemodynamics. Blood flow quantification and 3D hemodynamic visualization can be completed anywhere within the imaging volume to give unique perspectives of the complex fetal flow circuit, provided image quality is sufficient.

However, 4D flow MR requires collection of much larger datasets than 2D PC MR, and scan times become prohibitively long at the high spatial and temporal resolutions required for imaging of fetal heart vessels. While vendor-provided mitigation techniques such as parallel imaging reduce this requirement, the resulting scans are still too long, upwards of several minutes, for use in fetal imaging. Moreover, with these extended scan times, gross fetal motion becomes even more problematic.

FLOW ANALYSIS

Data corrections

Correction of background phase offsets caused by eddy currents are not commonly used in fetal cardiovascular 2D PC MR. One report of flows quantified with and without the correction showed little impact,[48] however, care should be taken as the correction itself could contribute error in some cases.[63]

Pre-processing corrections are typically applied in 4D flow MR For fetal imaging, these are often automatically applied before retrospective quantification and visualization. Background phase offsets require fitting of a 3D polynomial to the phase of static tissue,[64] and this semi-automatic step is incorporated into most commercial 4D flow MR processing software. As the amplitudes

of fetal flows vary significantly throughout the cardiac vasculature, exams are often performed with low velocity encoding (≤100 cm/s) to maximize velocity-to-noise ratio and quantitative accuracy and, consequently, velocity unwrapping needs to be performed. Due to the large data sets in 4D flow, this is often done with automatic techniques[65,66] and then visually inspected for further manual corrections.

Vessel contours

A region of interest is used to quantify blood flow within a vessel. Regions are typically generated using software tools with semi-automatic vessel contour detection that adapts the region to each phase of the cardiac cycle,[63] though a static contour may be sufficient for vessels that experience less movement and pulsation, like the DAo and UV.[48] Visual inspection and manual refinement can mitigate segmentation errors when automatic propagation is used to generate time-resolved vessel contours.[47] The contour should contain the entire vessel or be slightly larger to avoid significant flow underestimation errors that can occur with small regions.[48]

Indexed flows

Fetal flows are often indexed to fetal weight to remove a dependence on gestational age, since combined ventricular output in relation to fetal body weight is constant over the last two-thirds of gestation in healthy fetuses.[1] Fetal weight can be calculated by converting the body volume, estimated from segmentation of 2D or 3D steady-state free precession MRI data, using a conversion based on fetal density.[33,67,68]

Flow distribution

In some cases, flows that cannot be measured directly can instead be derived using flow volume continuity equations, based on the well-accepted assumption of incompressible blood in large vessels.[28,33] In normal fetal circulation (Figure 1), these equations are

$$Q_{SVC} = Q_{AAo} - (Q_{DAo} - Q_{DA})$$

$$Q_{MPA} = Q_{DA} + (Q_{LPA} + Q_{RPA}) \text{ and}$$

$$Q_{FO} + (Q_{RPA} + Q_{LPA}) = Q_{AAo} + Q_{CA}$$

where Q is flow, Q_{LPA} and Q_{RPA} are the flows in the left and right pulmonary arteries and Q_{CA} is the flow to the coronary arteries. Q_{LPA} and Q_{RPA} are sometimes combined as total pulmonary blood flow (PBF). Q_{CA} is assumed to be 3% of the combined ventricular output (CVO)[1] which is given by

$$Q_{CVO} = Q_{MPA} + Q_{AAo} + Q_{CA}$$

and can be calculated as

$$Q_{CVO} = (Q_{MPA} + Q_{AAo})/0.97$$

In congenital heart disease circulations, these equations may differ depending on subtype.[28]

Oxygen transport

Oxygen saturation measurements from MR oximetry[69,70] can be combined with flow to calculate oxygen transport as the product of flow and oxygen content.[71] Fetal oxygen consumption is the difference between oxygen transport in the umbilical vein and oxygen transport in the umbilical arteries. In the human, cerebral oxygen consumption is often obtained using superior vena cava as a surrogate for cerebral blood flow along with oxygen saturations in the AAo and SVC.[71]

4D flow visualization

A 3D segmentation of the vasculature of interest is commonly used to distinguish blood from background tissue and air in 4D flow MR. This segmentation is made from an angiographic image, which can be from a separate MRI scan such as contrast-enhanced MR angiography or time-of-flight angiography or calculated directly from 4D flow MR.[72]

Visualization options for the rich data contained in 4D flow MR include instantaneous streamlines, 3D velocity vector maps, isosurface mapping of parameters and pathlines.[73] For fetal representation, pathlines, which trace the paths of virtual particles through a time-dependent velocity field, permit the seeding of particles at a point of interest in the volume and following the tortuous blood routes through the fetal vasculature.

APPLICATIONS

Human studies

Healthy fetal circulation

Normal distribution of blood in late gestational age human fetus has been studied using cine PC MR.[28,33,45] In these investigations, flow was measured in the MPA, AAo, DA, DAo, SVC, UV and the branch pulmonary arteries, as in Figure 2. Flows from a recent study of 192 cases,[28] including 40 healthy fetuses, are shown in Figure 6 along with a model of the normal distribution of blood in Figure 7 which is in line with previous estimates based on ultrasound in humans and radionuclide-labeled microspheres in the fetal lamb.[1] MR oximetry was also used in the same study to assess oxygen transport throughout the fetal circulatory system. Other studies have reported the use of ungated 2D PC MR in the umbilical vein to estimate oxygen delivery[74] and 4D flow using relatively low spatial resolution to visualize aortic flow.[29]

Congenital heart disease

Cine 2D PC MR has been used to assess the redistribution of blood flow in human fetuses with various subtypes of congenital heart disease.[28,71,75,76] Overall, fetal organ perfusion was maintained in most subtypes of congenital heart disease despite obstructions leading to dramatic changes in other parts of the circulatory system. For example, SVC flow, a surrogate for cerebral blood flow, was generally at normal levels as shown in Figures 6 and 7. In fetuses with right heart obstructions, such as tetralogy of Fallot and tricuspid atresia, MPA and DA flows were reduced, as expected, and most of the systemic systems were supplied by an increase in blood flow through the AAo.[28]

Figure 6. Blood flow in the major vessels of normal controls and fetuses with cyanotic congenital heart disease. Scatter plots show (top) the distribution and group mean (bar) of flow normalized by fetal weight, and (bottom) group-wise difference plot with mean and 95% confidence interval for congenital heart disease subtypes compared to normal controls. Flows in congenital heart disease subtypes with confidence intervals that do not cross zero in the difference plot are significantly different from normal controls. Negative blood flows in the DA denote retrograde flow and left to right shunt in the FO. † Showing measured flows and, in cases with missing measurements, flows derived from other measurements. ‡ Showing derived flows exclusively. AAo, ascending aorta; CVO, combined ventricular output; DA, ductus arteriosus; DAo, descending aorta; EA, Ebstein's anomaly; FO, foramen ovale; HLH, hypoplastic left heart; MPA, main pulmonary artery; PBF, pulmonary blood flow; SVC, superior vena cava; TA, tricuspid atresia; TGA, transposition of the great arteries; TOF, tetralogy of Fallot; UV, umbilical vein. Reprinted with permission from Ultrasound Obstet Gynecol 2021; doi: 10.1002/uog.23707. Caption adapted from original.

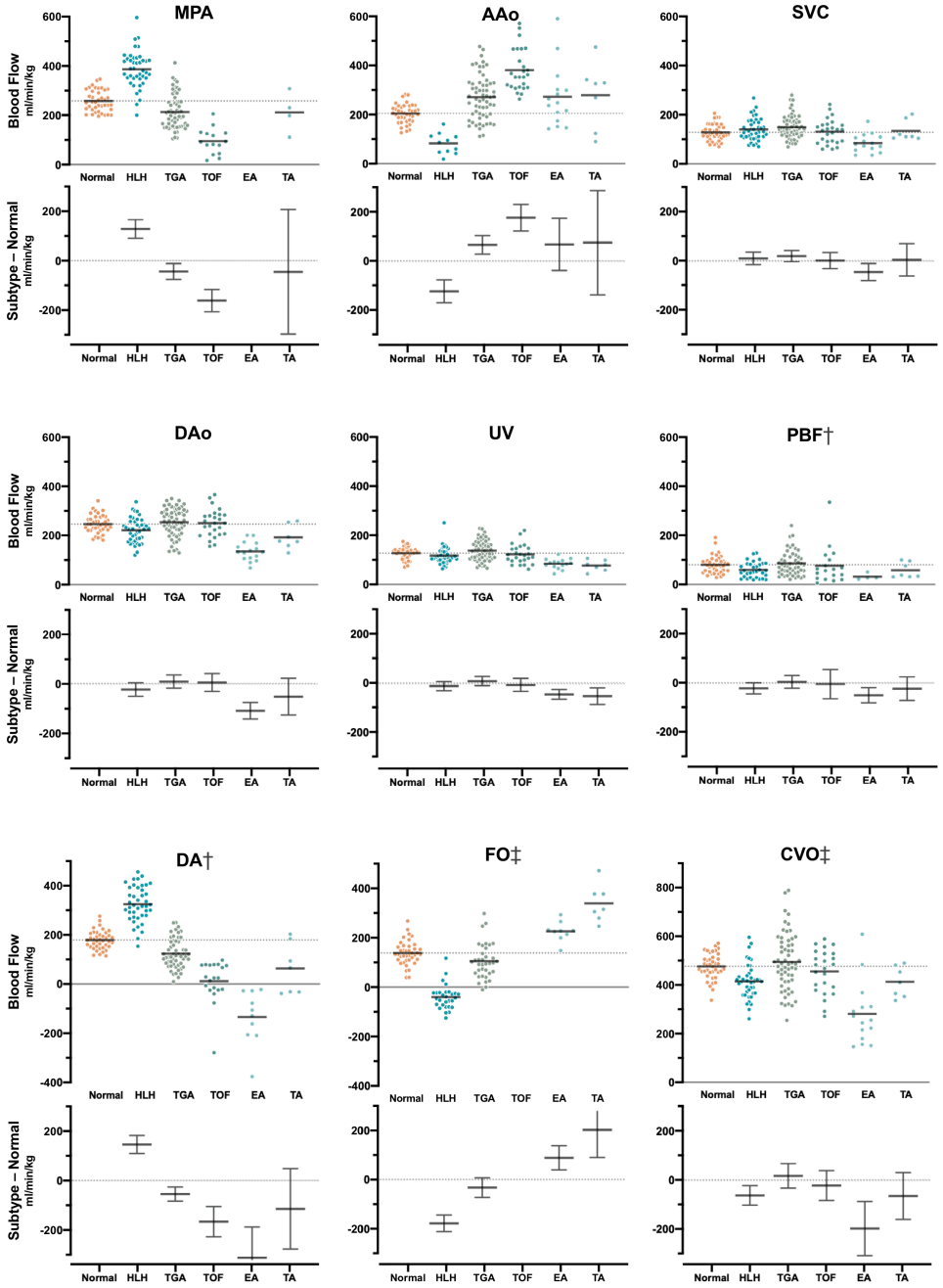

Conversely, in fetuses with hypoplastic left hearts, AAo flow was dramatically reduced and supply to the brain was provided by an increase in DA flow via retrograde flow through the aortic isthmus and arch.[28,75] Cerebral oxygen consumption was found to be lower in fetuses with congenital heart disease and associated with lower brain weight,[71] a predictor of neonatal brain development.[77,78] In a study of coarctation of the aorta, the combination of reduced flow in the ascending aorta in combination with

Figure 7. Distribution of blood flow in late gestation human fetuses with normal hearts and cyanotic congenital heart disease subtypes. Flows are shown as percentage of the combined ventricular output. Reported flows are based on median measured values subject to a constrained model ensuring continuity of flow volume throughout the fetal circulatory system. Negative values indicate retrograde flow or, in the case of the FO, left to right shunt. Shading indicates blood oxygen saturation measured by MR oximetry. AAo, ascending aorta; DA, ductus arteriosus; DAo, descending aorta; DV, ductus venosus; EA, Ebstein's anomaly; HLHS, hypoplastic left heart syndrome; IVC, inferior vena cava; LA, left atrium; LV, left ventricle; MPA, main pulmonary artery; PBF, pulmonary blood flow; RA, right atrium; RV, right ventricle; SVC, superior vena cava; TGA, transposition of the great arteries; UV, umbilical vein; UA, umbilical arteries. Figure and caption adapted with permission from Ultrasound Obstet Gynecol 2021; doi: 10.1002/uog.23707.

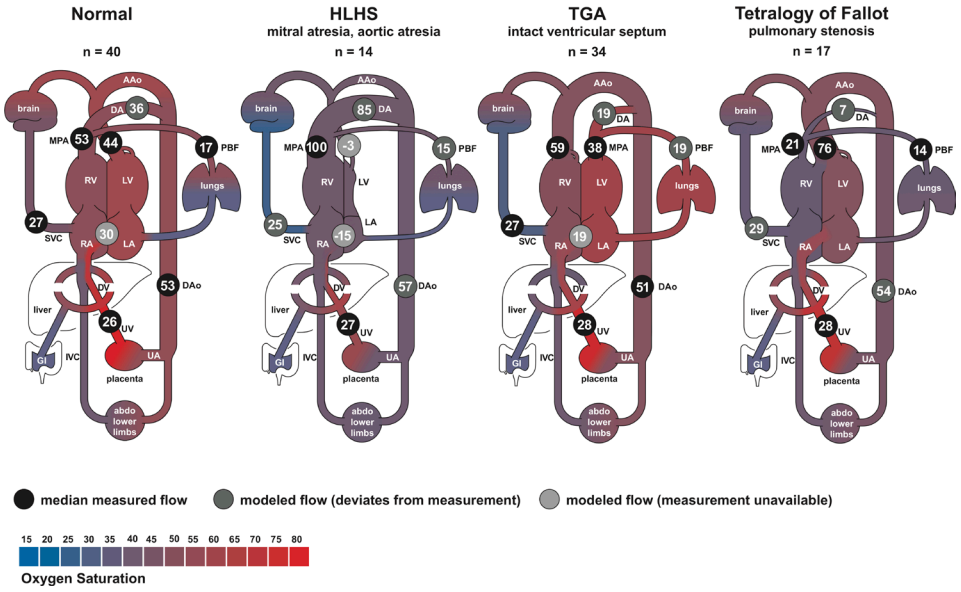

changes in arch anatomy in 3D MRI *in utero* was found to be predictive of the need for neonatal surgical repair.[68] Flow quantification with non-triggered 2D PC MR in fetuses with congenital heart disease has been limited,[79,80] but has been employed to reveal direction of blood flow to support diagnosis of left superior vena cava and anomalous pulmonary venous connections.[41] *In vitro* 4D flow MR in 3D printed phantom models of patient-specific fetal hearts with normal and hypoplastic left ventricle geometries has also been reported.[81]

Intrauterine growth restriction

A study of late-onset intrauterine growth restriction showed dramatically reduced fetal oxygen delivery due to placental insufficiency and lower brain weight Z scores on fetal and neonatal MRI.[82] In these fetuses, flows measured by cine 2D PC MR showed preferential flow to the brain with a reduction in pulmonary blood flow due to brain sparing physiological adaptations.

Interventions

PC MR in hypoplastic left heart fetuses with obstructed pulmonary venous drainage showed improved pulmonary blood flow to normal levels following fetal atrial stenting to decompress the left atrium and pulmonary veins.[75] Similarly, a reduction in retrograde DA flow was observed following treatment with transplacental non-steroidal anti-inflammatory drugs to control circular shunt in fetuses with Ebstein's anomaly.[79] Acute maternal hyperoxygenation has been shown to increase fetal oxygen delivery and lead to increased pulmonary blood flow due to pulmonary vasodilation in fetuses with congenital heart disease.[83]

Animal models

Preclinical sheep, pig, and macaque models of pregnancy have been used for decades to better characterize fetal physiology and anatomy throughout pregnancy.[84–88] Flow MRI has only been recently possible in these animal models thanks to the combination of surgically implanted, invasive pressure probes to reliably detect the fetal heart rate for use in cardiac gating[89] and the administration of anaesthesia to the mother and fetus to limit motion. The implanted pressure probe can also be used to sample blood throughout scanning to detect dynamic changes in fetal physiology. With animals prepared in this way, high resolution 2D PC MR has been demonstrated with good internal agreement at a number of vessel measurement locations in fetal sheep.[90,91] Similarly, with virtually no motion (aside from maternal breathing) and the capability of longer scan times, high resolution 4D flow MR is possible using scan lengths of 10–20 min. This has been demonstrated in large extracardiac vessels in fetal macaques[92] and the great vessels and hepatic vasculature in fetal sheep.[93,94] With 4D flow MR, the first ever *in vivo* 3D visualization and quantification of the streaming of oxygen- and nutrient-rich blood from the ductus venosus through the foramen ovale were demonstrated, as shown in Figures 8 and 9.

Combined with animal models of pregnancy, flow MRI techniques are now being used to explore targeted therapies for intrauterine growth restriction. Using 2D PC MR and 3D anatomical MRI, the fetal weight of growth restricted fetal sheep has been shown to increase after the administration of resveratrol, coupled with increasing uterine blood flow.[95] 4D flow MR, taken before and after

Figure 8. Particle traces from 4D flow MR in fetal sheep. (Top) Oblique ventral view of SVC (blue) and IVCp (red) return to the right side-of the heart, shown at four time points over two cardiac cycles. The MPA receives blood from both vessels, serving as a conduit to the lungs and lower body. The AAo only receives IVCp blood via right-to-left atrial shunting. (Bottom) Ventral view showing preferential delivery of DV blood to the left side of the heart. DV (red) and IVCd (blue) particles are shown at four time points over one cardiac cycle. The two streams remain well-separated, with blood from the DV primarily entering the left heart through the FO while IVCd remains in the right heart. SVC, superior vena cava; IVCp, proximal inferior vena cava; AAo, ascending aorta; MPA, main pulmonary artery; DV, ductus venosus; IVCd, distal inferior vena cava; FO, foramen ovale; RV, right ventricle; LV, left ventricle. Figure and caption adapted from *J Cardiovasc Magn Reson*. 2019; 21(1) under CC BY 4.0.

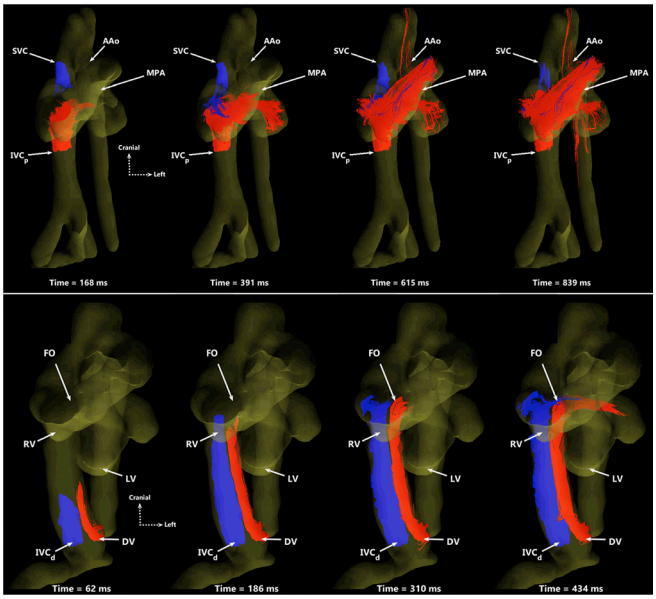

Figure 9. Right lateral view of the segmented fetal sheep vasculature for quantitation of blood flow volumes. Color-coded contours indicate locations of corresponding flow measurements at right. (Right) Blood flow *vs* cardiac time at all measurement locations, separated as (top) input to and (bottom) output from the heart. Cardiac inputs from the DV, IVCd, IVCp, and SVC display typical biphasic nature with greater pulsatility proximal to the heart, whereas UV flow appears nearly constant. Note UV flow was measured downstream from the junction of the typical two UVs found in fetal sheep. Outputs from the MPA, DA, AAo, BT, and DAo display large systolic peaks and low diastolic flows. BT and PBF display retrograde diastolic flow, likely indicative of runoff to the placenta through the aortic isthmus and DA. UV, umbilical vein; DV, ductus venosus; IVCd, distal inferior vena cava; IVCp, proximal inferior vena cava; SVC, superior vena cava; FO, foramen ovale; AAo, ascending aorta; BT, brachiocephalic trunk; DA, ductus arteriosus; DAo, descending aorta; MPA, main pulmonary artery; PBF, combined pulmonary blood flow. Reprinted from *J Cardiovasc Magn Reson*. 2019; 21(1) under CC BY 4.0. Caption adapted from original.

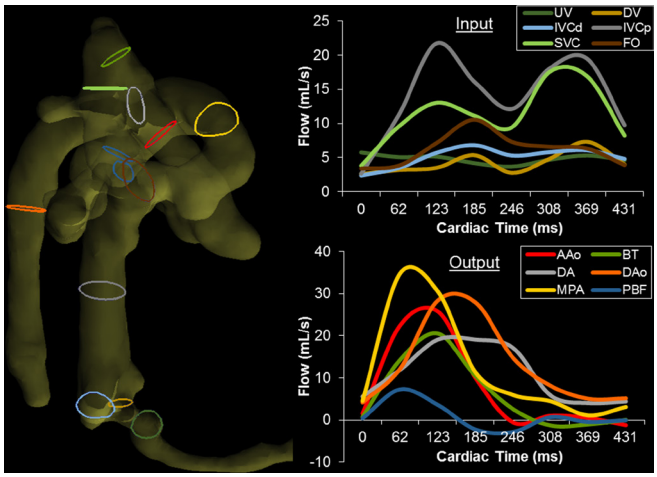

prostaglandin I_2 injection, has been used to examine drug effects on ductal tone and flow physiology.[96] Taken together, these studies enhance understanding of fetal cardiovascular physiology and help to inform translation of techniques and potential interventions to human subjects.

DISCUSSION

Strengths and limitations

Cine PC MR is the gold-standard for cardiovascular flow measurements in the post-natal population. With novel solutions to the unique challenges of fetal cardiovascular MR, cine PC MR has been shown to be feasible and reliable for characterizing healthy late-gestation fetal circulation as well as circulations disrupted by congenital heart disease or intrauterine growth restriction. However, prescription of imaging planes cross-sectional to each vessel of interest can be challenging, and fetal and maternal motion can impact data quality if uncorrected. Additionally, gating solutions require additional hardware or post-processing software.

4D flow in animal models has provided visualizations of the complex streaming of blood that occurs in the fetal circulation (Figure 8) as well as a capacity for flow volume quantification at any location in the acquired volume (Figure 9). However, in human studies without the aid of anesthetics to allow for long scan durations, 4D flow has been limited.

Outlook

Slice-to-volume (SVR) reconstructions, commonly used in fetal brain MRI, have been extended to visualize the human fetal heart.[97,98] The SVR framework uses multiple 2D acquisitions covering the anatomy of interest that are combined as a single volume in the image domain using scattered data interpolation and super-resolution methods with retrospective 3D motion correction. Recent works demonstrate that SVR is capable of generating human fetal cardiovascular 4D flow volumes, either from motion-corrected fully encoded radial cine PC MR[99] or real-time balance steady-state free precession images using the inherent velocity sensitivity in the phase images.[98,100] These methods are a potential route to motion-robust visualization and quantification of blood flow throughout the fetal cardiovascular system.

4D flow MR can provide whole-heart coverage without the need for challenging 2D scan plane prescription during acquisition. Such data can be used for retrospective assessment of flow distribution as well as morphology and function. In the future, fetal flow imaging with volumetric coverage may be incorporated in human studies, either through further development of SVR methods or by employing higher acceleration rates and motion-corrected methods to achieve shorter, high resolution conventional 4D flow MR.

2D PC MR has been the most used technique for fetal flow imaging and will likely see broader adoption as gating solutions become more readily available and usable. Incorporating rapid imaging with non-Cartesian trajectories will improve robustness to motion and accuracy of flow measurements in examinations of human fetuses. With continued development towards fetal therapies that require sophisticated fetal imaging technology, the techniques of fetal cardiovascular flow MR could play an increasingly important role in diagnosis and treatment monitoring.

REFERENCES

1. Yagel S, Silverman NH, Gembruch U, eds. Circulation in the normal fetus and cardiovascular adaptations to birth. *Fetal Cardiology* 2019; 119–37. Available from: https://doi.org/10.1201/9780429461118-16. doi: https://doi.org/10.1201/9780429461118-16
2. Rudolph A. *Fetal Cardiology*. 3rd ed. CRC Press; 2019., pp.708–22. Available from: https://doi.org/10.1201/9780429461118-61. doi: https://doi.org/10.1201/9780429461118-61
3. Peyvandi S, Donofrio MT. Circulatory changes and cerebral blood flow and oxygenation during transition in newborns with congenital heart disease. *Semin Pediatr Neurol* 2018; **28**: 38–47. https://doi.org/10.1016/j.spen.2018.05.005
4. Donofrio MT, Moon-Grady AJ, Hornberger LK, Copel JA, Sklansky MS, Abuhamad A, et al. Diagnosis and treatment of fetal cardiac disease: A scientific statement from the american heart association. *Circulation* 2014; **129**: 2183–2242. https://doi.org/10.1161/01.cir.0000437597.44550.5d
5. Gill RW. Measurement of blood flow by ultrasound: accuracy and sources of error. *Ultrasound Med Biol* 1985; **11**: 625–41. https://doi.org/10.1016/0301-5629(85)90035-3
6. Schmidt KG, Di Tommaso M, Silverman NH, Rudolph AM. Doppler echocardiographic assessment of fetal descending aortic and umbilical blood flows. validation studies in fetal lambs. *Circulation* 1991; **83**: 1731–37. https://doi.org/10.1161/01.CIR.83.5.1731
7. Hoyt K, Hester FA, Bell RL, Lockhart ME, Robbin ML. Accuracy of volumetric flow rate measurements. *Journal of Ultrasound in Medicine* 2009; **28**: 1511–18. https://doi.org/10.7863/jum.2009.28.11.1511
8. Park MY, Jung SE, Byun JY, Kim JH, Joo GE. Effect of beam-flow angle on velocity measurements in modern doppler ultrasound systems. *American Journal of Roentgenology* 2012; **198**: 1139–43. https://doi.org/10.2214/AJR.11.7475
9. Blanco P. Volumetric blood flow measurement using doppler ultrasound: concerns about the technique. *J Ultrasound* 2015; **18**: 201–4. https://doi.org/10.1007/s40477-015-0164-3
10. Adriaanse BME, van Vugt JMG, Haak MC. Three- and four-dimensional ultrasound in fetal echocardiography: an up-to-date overview. *J Perinatol* 2016; **36**: 685–93. https://doi.org/10.1038/jp.2016.23
11. Dave JK, Mc Donald ME, Mehrotra P, Kohut AR, Eisenbrey JR, Forsberg F. Recent technological advancements in cardiac ultrasound imaging. *Ultrasonics* 2018; **84**: 329–40. https://doi.org/10.1016/j.ultras.2017.11.013
12. Nyrnes SA, Fadnes S, Wigen MS, Mertens L, Lovstakken L. Blood speckle-tracking based on high-frame rate ultrasound imaging in pediatric cardiology. *J Am Soc Echocardiogr* 2020; **33**: 493–503. https://doi.org/10.1016/j.echo.2019.11.003
13. Simpson J, Zidere V, Miller OI. *Fetal Cardiology*. Cham: Springer International Publishing; 2018., pp.189–97. https://doi.org/10.1007/978-3-319-77461-9
14. Roy CW, van Amerom JFP, Marini D, Seed M, Macgowan CK. Fetal cardiac MRI: A review of technical advancements. *Top Magn Reson Imaging* 2019; **28**: 235–44. https://doi.org/10.1097/RMR.0000000000000218
15. van Amerom J D, Saini BS, Sun L, Seed M. MR imaging of the fetal heart. 2020..
16. Jensen A, Berger R. Fetal circulatory responses to oxygen lack. *J Dev Physiol* 1991; **16**: 181–207.
17. Schneider C, McCrindle BW, Carvalho JS, Hornberger LK, McCarthy KP, Daubeney PEF. Development of Z-scores for fetal cardiac dimensions from echocardiography. *Ultrasound Obstet Gynecol* 2005; **26**: 599–605. https://doi.org/10.1002/uog.2597
18. Ruano R, de Fátima Yukie Maeda M, Niigaki JI, Zugaib M. Pulmonary artery diameters in healthy fetuses from 19 to 40 weeks' gestation. *J Ultrasound Med* 2007; **26**: 309–16. https://doi.org/10.7863/jum.2007.26.3.309
19. Nowak D, Kozłowska H, Żurada A, Gielecki J. Diameter of the ductus arteriosus as a predictor of patent ductus arteriosus (PDA). *Open Medicine* 2011; **6**: 418–24. https://doi.org/10.2478/s11536-011-0047-8
20. Pildner von Steinburg S, Boulesteix A-L, Lederer C, Grunow S, Schiermeier S, Hatzmann W, et al. What is the "normal" fetal heart rate? *PeerJ* 2013; **1**: e82. https://doi.org/10.7717/peerj.82
21. Jansz MS, Seed M, van Amerom JFP, Wong D, Grosse-Wortmann L, Yoo S-J, et al. Metric optimized gating for fetal cardiac MRI. *Magn Reson Med* 2010; **64**: 1304–14. https://doi.org/10.1002/mrm.22542
22. Goolaub DS, Roy CW, Schrauben E, Sussman D, Marini D, Seed M, et al. Multidimensional fetal flow imaging with cardiovascular magnetic resonance: A feasibility study. *J Cardiovasc Magn Reson* 2018; **20**: 77. https://doi.org/10.1186/s12968-018-0498-z
23. Kording F, Schoennagel BP, de Sousa MT, Fehrs K, Adam G, Yamamura J, et al. Evaluation of a portable doppler ultrasound gating device for fetal cardiac MR imaging: initial results at 1.5T and 3T. *MRMS* 2018; **17**: 308–17. https://doi.org/10.2463/mrms.mp.2017-0100
24. Kording F, Yamamura J, de Sousa MT, Ruprecht C, Hedström E, Aletras AH, et al. Dynamic fetal cardiovascular magnetic resonance imaging using doppler ultrasound gating. *J Cardiovasc Magn Reson* 2018; **20**: 17. https://doi.org/10.1186/s12968-018-0440-4
25. Crowe LA, Manasseh G, Chmielewski A, Hachulla A-L, Speicher D, Greiser A, et al. Spatially resolved MR-compatible doppler ultrasound: proof of concept for triggering of diagnostic quality cardiovascular MRI for function and flow quantification at 3T. *IEEE Trans Biomed Eng* 2018; **65**: 294–306. https://doi.org/10.1109/TBME.2017.2764111

26. Roy CW, Seed M, Kingdom JC, Macgowan CK. Motion compensated cine CMR of the fetal heart using radial undersampling and compressed sensing. *J Cardiovasc Magn Reson* 2017; **19**: 29. https://doi.org/10.1186/s12968-017-0346-6
27. van Amerom JFP, Lloyd DFA, Price AN, Kuklisova Murgasova M, Aljabar P, Malik SJ, et al. Fetal cardiac cine imaging using highly accelerated dynamic MRI with retrospective motion correction and outlier rejection. *Magn Reson Med* 2018; **79**: 327–38. https://doi.org/10.1002/mrm.26686
28. Sun L, van Amerom JFP, Marini D, Portnoy S, Lee F-T, Saini BS, et al. MRI characterization of hemodynamic patterns of human fetuses with cyanotic congenital heart disease. *Ultrasound Obstet Gynecol* 2021; **58**: 824–36. https://doi.org/10.1002/uog.23707
29. Tavares de Sousa M, Hecher K, Kording F, Yamamura J, Lenz A, Adam G, et al. Fetal dynamic magnetic resonance imaging using doppler ultrasound gating for the assessment of the aortic isthmus: A feasibility study. *Acta Obstet Gynecol Scand* 2020; **100**: 67–73. https://doi.org/10.1111/aogs.13957
30. Tang C, Blatter DD, Parker DL. Accuracy of phase-contrast flow measurements in the presence of partial-volume effects. *J Magn Reson Imaging* 1993; **3**: 377–85. https://doi.org/10.1002/jmri.1880030213
31. Cibis M, Potters WV, Gijsen FJ, Marquering H, van Ooij P, vanBavel E, et al. The effect of spatial and temporal resolution of cine phase contrast MRI on wall shear stress and oscillatory shear index assessment. *PLoS One* 2016; **11**(9): e0163316. https://doi.org/10.1371/journal.pone.0163316
32. Santini F, Pansini M, Hrabak-Paar M, Yates D, Langenickel TH, Bremerich J, et al. On the optimal temporal resolution for phase contrast cardiovascular magnetic resonance imaging: establishment of baseline values. *J Cardiovasc Magn Reson* 2020; **22**: 72. https://doi.org/10.1186/s12968-020-00669-1
33. Seed M, F P van Amerom J, Yoo S-J, Al Nafisi B, Grosse-Wortmann L, Jaeggi E, et al. Feasibility of quantification of the distribution of blood flow in the normal human fetal circulation using CMR: a cross-sectional study. *J Cardiovasc Magn Reson* 2012; **14**: 79. https://doi.org/10.1186/1532-429X-14-79
34. Bidhult S, Töger J, Heiberg E, Carlsson M, Arheden H, Aletras AH, et al. Independent validation of metric optimized gating for fetal cardiovascular phase-contrast flow imaging. *Magn Reson Med* 2019; **81**: 495–503. https://doi.org/10.1002/mrm.27392
35. Machado-Rivas F, Jaimes C, Kirsch JE, Gee MS. Image-quality optimization and artifact reduction in fetal magnetic resonance imaging. *Pediatr Radiol* 2020; **50**: 1830–38. https://doi.org/10.1007/s00247-020-04672-7
36. Nagaraj UD, Calvo-Garcia MA, Merrow AC, Zhang B, Tkach JA, Kline-Fath BM. Utilization of 3-T fetal magnetic resonance imaging in clinical practice: a single-institution experience. *Pediatr Radiol* 2021; **51**: 1798–1808. https://doi.org/10.1007/s00247-021-05087-8
37. Colleran GC, Kyncl M, Garel C, Cassart M. Fetal magnetic resonance imaging at 3 tesla — the european experience. *Pediatr Radiol* 2022; **52**: 959–70. https://doi.org/10.1007/s00247-021-05267-6
38. Gholipour A, Estroff JA, Barnewolt CE, Robertson RL, Grant PE, Gagoski B, et al. Fetal MRI: A technical update with educational aspirations. *Concepts Magn Reson* 2014; **43**: 237–66. https://doi.org/10.1002/cmr.a.21321
39. Tsai-Goodman B, Zhu MY, Al-Rujaib M, Seed M, Macgowan CK. Foetal blood flow measured using phase contrast cardiovascular magnetic resonance – preliminary data comparing 1.5 T with 3.0 T. *J Cardiovasc Magn Reson* 2015; **17**: 30. https://doi.org/10.1186/s12968-015-0132-2
40. Hata N, Wada T, Kashima K, Okada Y, Unno N, Kitagawa M, et al. Non-gated fetal MRI of umbilical blood flow in an acardiac twin. *Pediatr Radiol* 2005; **35**: 826–29. https://doi.org/10.1007/s00247-005-1454-2
41. Dong S-Z, Zhu M, Ji H, Ren J-Y, Liu K. Fetal cardiac MRI: a single center experience over 14-years on the potential utility as an adjunct to fetal technically inadequate echocardiography. *Sci Rep* 2020; **10**: 12373. https://doi.org/10.1038/s41598-020-69375-3
42. Krishnamurthy U, Yadav BK, Jella PK, Haacke EM, Hernandez-Andrade E, Mody S, et al. Quantitative flow imaging in human umbilical vessels in utero using nongated 2d phase contrast mri. *J Magn Reson Imaging* 2018; **48**: 283–89. https://doi.org/10.1002/jmri.25917
43. Bakker CJ, Kouwenhoven M, Hartkamp MJ, Hoogeveen RM, Mali WP. Accuracy and precision of time-averaged flow as measured by nontriggered 2D phase-contrast MR angiography, a phantom evaluation. *Magn Reson Imaging* 1995; **13**: 959–65. https://doi.org/10.1016/0730-725x(95)02005-e
44. Hangiandreou NJ, Rossman PJ, Riederer SJ. Analysis of MR phase-contrast measurements of pulsatile velocity waveforms. *J Magn Reson Imaging* 1993; **3**: 387–94. https://doi.org/10.1002/jmri.1880030214
45. Prsa M, Sun L, van Amerom J, Yoo S-J, Grosse-Wortmann L, Jaeggi E, et al. Reference ranges of blood flow in the major vessels of the normal human fetal circulation at term by phase-contrast magnetic resonance imaging. *Circ Cardiovasc Imaging* 2014; **7**: 663–70. https://doi.org/10.1161/CIRCIMAGING.113.001859
46. Schoennagel BP, Remus CC, Yamamura J, Kording F, Tavares de Sousa M, de Sousa MT, et al. Fetal blood flow velocimetry by phase-contrast MRI using A new triggering method and comparison with doppler ultrasound in A sheep model: A pilot study. *MAGMA* 2014; **27**: 237–44. https://doi.org/10.1007/s10334-013-0397-0
47. Schoennagel BP, Yamamura J, Kording F, Fischer R, Bannas P, Adam G, et al. Fetal dynamic phase-contrast MR angiography using ultrasound gating and comparison with doppler ultrasound measurements. *Eur Radiol* 2019; **29**: 4169–76. https://doi.org/10.1007/s00330-018-5940-y
48. Ryd D, Sun L, Steding-Ehrenborg K, Bidhult S, Kording F, Ruprecht C, et al. Quantification of blood flow in the fetus with cardiovascular magnetic resonance imaging using doppler ultrasound gating: validation against metric optimized gating. *J Cardiovasc Magn Reson* 2019; **21**: 74. https://doi.org/10.1186/s12968-019-0586-8
49. Goolaub DS, Xu J, Schrauben E, Sun L, Roy CW, Marini D, et al. fetal flow quantification in great vessels using motion-corrected radial phase contrast MRI : comparison with cartesian . *J Magn Reson Imaging* 2020; **53**: 540–51. https://doi.org/10.1002/jmri.27334
50. Schulz A, Lloyd DFA, van Poppel MPM, Roberts TA, Steinweg JK, Pushparajah K, et al. Structured analysis of the impact of fetal motion on phase-contrast MRI flow measurements with metric optimized gating. *Sci Rep* 2022; **12**: 1–11. https://doi.org/10.1038/s41598-022-09327-1
51. Feng L, Grimm R, Block KT, Chandarana H, Kim S, Xu J, et al. Golden-angle radial sparse parallel MRI: combination of compressed sensing, parallel imaging, and golden-angle radial sampling for fast and flexible dynamic volumetric MRI. *Magn Reson Med* 2014; **72**: 707–17. https://doi.org/10.1002/mrm.24980
52. Goolaub DS, Marini D, Seed M, Macgowan CK. Human fetal blood flow quantification with magnetic resonance imaging and motion compensation. *J Vis Exp* 2021; : 1–13. https://doi.org/10.3791/61953
53. Malamateniou C, Malik SJ, Counsell SJ, Allsop JM, McGuinness AK, Hayat T, et al. Motion-compensation techniques in neonatal and fetal MR imaging. *AJNR Am J*

Neuroradiol 2013; **34**: 1124–36. https://doi.org/10.3174/ajnr.A3128
54. Markl M, Frydrychowicz A, Kozerke S, Hope M, Wieben O. 4D flow MRI. *J Magn Reson Imaging* 2012; **36**: 1015–36. https://doi.org/10.1002/jmri.23632
55. Hope MD, Hope TA, Crook SES, Ordovas KG, Urbania TH, Alley MT, et al. 4D flow CMR in assessment of valve-related ascending aortic disease. *JACC Cardiovasc Imaging* 2011; **4**: 781–87. https://doi.org/10.1016/j.jcmg.2011.05.004
56. Ma LE, Vali A, Blanken C, Barker AJ, Malaisrie C, McCarthy P, et al. Altered aortic 3-dimensional hemodynamics in patients with functionally unicuspid aortic valves. *Circ Cardiovasc Imaging* 2018; **11**(8): e007915. https://doi.org/10.1161/CIRCIMAGING.118.007915
57. Robinson JD, Rose MJ, Joh M, Jarvis K, Schnell S, Barker AJ, et al. 4-D flow magnetic-resonance-imaging-derived energetic biomarkers are abnormal in children with repaired tetralogy of fallot and associated with disease severity. *Pediatr Radiol* 2019; **49**: 308–17. https://doi.org/10.1007/s00247-018-4312-8
58. Elsayed A, Gilbert K, Scadeng M, Cowan BR, Pushparajah K, Young AA. Four-dimensional flow cardiovascular magnetic resonance in tetralogy of fallot: a systematic review. *J Cardiovasc Magn Reson* 2021; **23**: 59. https://doi.org/10.1186/s12968-021-00745-0
59. Guala A, Teixido-Tura G, Dux-Santoy L, Granato C, Ruiz-Muñoz A, Valente F, et al. Decreased rotational flow and circumferential wall shear stress as early markers of descending aorta dilation in marfan syndrome: A 4D flow CMR study. *J Cardiovasc Magn Reson* 2019; **21**: 63. https://doi.org/10.1186/s12968-019-0572-1
60. Geiger J, Hirtler D, Gottfried K, Rahman O, Bollache E, Barker AJ, et al. Longitudinal evaluation of aortic hemodynamics in marfan syndrome: new insights from a 4D flow cardiovascular magnetic resonance multi-year follow-up study. *J Cardiovasc Magn Reson* 2017; **19**: 33. https://doi.org/10.1186/s12968-017-0347-5
61. Hsiao A, Lustig M, Alley MT, Murphy M, Chan FP, Herfkens RJ, et al. Rapid pediatric cardiac assessment of flow and ventricular volume with compressed sensing parallel imaging volumetric cine phase-contrast MRI. *American Journal of Roentgenology* 2012; **198**: W250–59. https://doi.org/10.2214/AJR.11.6969
62. Gabbour M, Schnell S, Jarvis K, Robinson JD, Markl M, Rigsby CK. 4-D flow magnetic resonance imaging: blood flow quantification compared to 2-D phase-contrast magnetic resonance imaging and doppler echocardiography. *Pediatr Radiol* 2014; **45**: 804–13. https://doi.org/10.1007/s00247-014-3246-z
63. Lotz J, Meier C, Leppert A, Galanski M. Cardiovascular flow measurement with phase-contrast MR imaging: basic facts and implementation. *RadioGraphics* 2002; **22**: 651–71. https://doi.org/10.1148/radiographics.22.3.g02ma11651
64. Walker PG, Cranney GB, Scheidegger MB, Waseleski G, Pohost GM, Yoganathan AP. Semiautomated method for noise reduction and background phase error correction in MR phase velocity data. *J Magn Reson Imaging* 1993; **3**: 521–30. https://doi.org/10.1002/jmri.1880030315
65. Xiang QS. Temporal phase unwrapping for cine velocity imaging. *J Magn Reson Imaging* 1995; **5**: 529–34. https://doi.org/10.1002/jmri.1880050509
66. Loecher M, Schrauben E, Johnson KM, Wieben O. Phase unwrapping in 4D MR flow with a 4D single-step laplacian algorithm. *J Magn Reson Imaging* 2016; **43**: 833–42. https://doi.org/10.1002/jmri.25045
67. Baker PN, Johnson IR, Gowland PA, Hykin J, Harvey PR, Freeman A, et al. Fetal weight estimation by echo-planar magnetic resonance imaging. *Lancet* 1994; **343**: 644–45. https://doi.org/10.1016/s0140-6736(94)92638-7
68. Lloyd DFA, van Poppel MPM, Pushparajah K, Vigneswaran TV, Zidere V, Steinweg J, et al. Analysis of 3-dimensional arch anatomy, vascular flow, and postnatal outcome in cases of suspected coarctation of the aorta using fetal cardiac magnetic resonance imaging. *Circ Cardiovasc Imaging* 2021; **14**: e012411: 1–11: . https://doi.org/10.1161/CIRCIMAGING.121.012411
69. Portnoy S, Seed M, Sled JG, Macgowan CK. Non-invasive evaluation of blood oxygen saturation and hematocrit from T_1 and T_2 relaxation times: in-vitro validation in fetal blood. *Magn Reson Med* 2017; **78**: 2352–59. https://doi.org/10.1002/mrm.26599
70. Saini BS, Darby JRT, Portnoy S, Sun L, Amerom J, Lock MC, et al. Normal human and sheep fetal vessel oxygen saturations by T2 magnetic resonance imaging. *J Physiol* 2020; **598**: 3259–81. https://doi.org/10.1113/JP279725
71. Sun L, Macgowan CK, Sled JG, Yoo S-J, Manlhiot C, Porayette P, et al. Reduced fetal cerebral oxygen consumption is associated with smaller brain size in fetuses with congenital heart disease. *Circulation* 2015; **131**: 1313–23. https://doi.org/10.1161/CIRCULATIONAHA.114.013051
72. Dumoulin CL, Souza SP, Walker MF, Wagle W. Three-dimensional phase contrast angiography. *Magn Reson Med* 1989; **9**: 139–49. https://doi.org/10.1002/mrm.1910090117
73. Dyverfeldt P, Bissell M, Barker AJ, Bolger AF, Carlhäll C-J, Ebbers T, et al. 4D flow cardiovascular magnetic resonance consensus statement. *J Cardiovasc Magn Reson* 2015; **17**: 72. https://doi.org/10.1186/s12968-015-0174-5
74. Rodríguez-Soto AE, Langham MC, Abdulmalik O, Englund EK, Schwartz N, Wehrli FW. MRI quantification of human fetal o_2 delivery rate in the second and third trimesters of pregnancy. *Magn Reson Med* 2018; **80**: 1148–57. https://doi.org/10.1002/mrm.27094
75. Al Nafisi B, van Amerom JFP, Forsey J, Jaeggi E, Grosse-Wortmann L, Yoo S-J, et al. Fetal circulation in left-sided congenital heart disease measured by cardiovascular magnetic resonance: a case-control study. *J Cardiovasc Magn Reson* 2013; **15**: 65. https://doi.org/10.1186/1532-429X-15-65
76. Porayette P, van Amerom JFP, Yoo S-J, Jaeggi E, Macgowan CK, Seed M. MRI shows limited mixing between systemic and pulmonary circulations in foetal transposition of the great arteries: a potential cause of in utero pulmonary vascular disease. *Cardiol Young* 2015; **25**: 737–44. https://doi.org/10.1017/S1047951114000870
77. Sadhwani A, Wypij D, Rofeberg V, Gholipour A, Mittleman M, Rohde J, et al. Fetal brain volume predicts neurodevelopment in congenital heart disease. *Circulation* 2022; **145**: 1108–19. https://doi.org/10.1161/CIRCULATIONAHA.121.056305
78. Kelly CJ, Makropoulos A, Cordero-Grande L, Hutter J, Price A, Hughes E, et al. Impaired development of the cerebral cortex in infants with congenital heart disease is correlated to reduced cerebral oxygen delivery. *Sci Rep* 2017; **7**(1): 15088. https://doi.org/10.1038/s41598-017-14939-z
79. Torigoe T, Mawad W, Seed M, Ryan G, Marini D, Golding F, et al. Treatment of fetal circular shunt with non-steroidal anti-inflammatory drugs. *Ultrasound Obstet Gynecol* 2019; **53**: 841–46. https://doi.org/10.1002/uog.20169
80. Tsuritani M, Morita Y, Miyoshi T, Kurosaki K, Yoshimatsu J. Fetal cardiac functional assessment by fetal heart magnetic resonance imaging. *J Comput Assist Tomogr* 2019; **43**: 104–8. https://doi.org/10.1097/RCT.0000000000000781

81. Ruedinger KL, Zhou H, Trampe B, Heiser T, Srinivasan S, Iruretagoyena JI, et al. Modeling fetal cardiac anomalies from prenatal echocardiography with 3-dimensional printing and 4-dimensional flow magnetic resonance imaging. *Circ Cardiovasc Imaging* 2018; **11**(9): e007705. https://doi.org/10.1161/CIRCIMAGING.118.007705
82. Zhu MY, Milligan N, Keating S, Windrim R, Keunen J, Thakur V, et al. The hemodynamics of late-onset intrauterine growth restriction by MRI. *Am J Obstet Gynecol* 2016; **214**: 367. https://doi.org/10.1016/j.ajog.2015.10.004
83. Porayette P, Madathil S, Sun L, Jaeggi E, Grosse-Wortmann L, Yoo S-J, et al. MRI reveals hemodynamic changes with acute maternal hyperoxygenation in human fetuses with and without congenital heart disease. *Prenat Diagn* 2016; **36**: 274–81. https://doi.org/10.1002/pd.4762
84. Rudolph AM, Heymann MA. The circulation of the fetus in utero. *Circulation Research* 1967; **21**: 163–84. https://doi.org/10.1161/01.RES.21.2.163
85. Edelstone DI, Rudolph AM. Preferential streaming of ductus venosus blood to the brain and heart in fetal lambs. *Am J Physiol* 1979; **237**: H724-9. https://doi.org/10.1152/ajpheart.1979.237.6.H724
86. Reynolds LP, Ford SP, Ferrell CL. Blood flow and steroid and nutrient uptake of the gravid uterus and fetus of sows. *J Anim Sci* 1985; **61**: 968–74. https://doi.org/10.2527/jas1985.614968x
87. Brüssow K-P, Kurth J, Vernunft A, Becker F, Tuchscherer A, Kanitz W. Laparoscopy guided doppler ultrasound measurement of fetal blood flow indices during early to mid-gestation in pigs. *J Reprod Dev* 2012; **58**: 243–47. https://doi.org/10.1262/jrd.11-059t
88. Golos TG, Bondarenko GI, Dambaeva SV, Breburda EE, Durning M. On the role of placental major histocompatibility complex and decidual leukocytes in implantation and pregnancy success using non-human primate models. *Int J Dev Biol* 2010; **54**: 431–43. https://doi.org/10.1387/ijdb.082797tg
89. Yamamura J, Schnackenburg B, Kooijmann H, Frisch M, Hecher K, Adam G, et al. High resolution MR imaging of the fetal heart with cardiac triggering: a feasibility study in the sheep fetus. *Eur Radiol* 2009; **19**: 2383–90. https://doi.org/10.1007/s00330-009-1420-8
90. Duan AQ, Darby JRT, Soo JY, Lock MC, Zhu MY, Flynn LV, et al. Feasibility of phase-contrast cine magnetic resonance imaging for measuring blood flow in the sheep fetus. *American Journal of Physiology-Regulatory, Integrative and Comparative Physiology* 2019; **317**: R780–92. https://doi.org/10.1152/ajpregu.00273.2017
91. Cho SKS, Darby JRT, Saini BS, Lock MC, Holman SL, Lim JM, et al. Feasibility of ventricular volumetry by cardiovascular MRI to assess cardiac function in the fetal sheep. *J Physiol* 2020; **598**: 2557–73. https://doi.org/10.1113/JP279054
92. Macdonald JA, Corrado PA, Nguyen SM, Johnson KM, Francois CJ, Magness RR, et al. Uteroplacental and fetal 4D flow MRI in the pregnant rhesus macaque. *J Magn Reson Imaging* 2019; **49**: 534–45. https://doi.org/10.1002/jmri.26206
93. Schrauben EM, Saini BS, Darby JRT, Soo JY, Lock MC, Stirrat E, et al. Fetal hemodynamics and cardiac streaming assessed by 4D flow cardiovascular magnetic resonance in fetal sheep. *J Cardiovasc Magn Reson* 2019; **21**: 8. https://doi.org/10.1186/s12968-018-0512-5
94. Schrauben EM, Darby JRT, Saini BS, Holman SL, Lock MC, Perumal SR, et al. Technique for comprehensive fetal hepatic blood flow assessment in sheep using 4D flow MRI. *J Physiol* 2020; **598**: 3555–67. https://doi.org/10.1113/JP279631
95. Aujla T, Darby JRT, Saini BS, Lock MC, Holman SL, Bradshaw EL, et al. Impact of resveratrol-mediated increase in uterine artery blood flow on fetal haemodynamics, blood pressure and oxygenation in sheep. *Exp Physiol* 2021; **106**: 1166–80. https://doi.org/10.1113/EP089237
96. Darby JRT, Schrauben EM, Saini BS, Holman SL, Perumal SR, Seed M, et al. Umbilical vein infusion of prostaglandin i_2 increases ductus venosus shunting of oxygen-rich blood but does not increase cerebral oxygen delivery in the fetal sheep. *J Physiol* 2020; **598**: 4957–67. https://doi.org/10.1113/JP280019
97. Lloyd DFA, Pushparajah K, Simpson JM, van Amerom JFP, van Poppel MPM, Schulz A, et al. Three-dimensional visualisation of the fetal heart using prenatal MRI with motion-corrected slice-volume registration: a prospective, single-centre cohort study. *Lancet* 2019; **393**: 1619–27. https://doi.org/10.1016/S0140-6736(18)32490-5
98. van Amerom JFP, Lloyd DFA, Deprez M, Price AN, Malik SJ, Pushparajah K, et al. Fetal whole-heart 4D imaging using motion-corrected multi-planar real-time MRI. *Magn Reson Med* 2019; **82**: 1055–72. https://doi.org/10.1002/mrm.27798
99. Goolaub DS, Xu J, Schrauben E, Marini D, Kingdom J, Sled J, et al. Volumetric Fetal Flow Imaging with Magnetic Resonance Imaging. August 9, 2021. https://doi.org/10.36227/techrxiv.15112944.v1
100. Roberts TA, van Amerom JFP, Uus A, Lloyd DFA, van Poppel MPM, Price AN, et al. Fetal whole heart blood flow imaging using 4D cine MRI. *Nat Commun* 2020; **11**(1): 4992. https://doi.org/10.1038/s41467-020-18790-1